Agrivoltaic Farm Design: Vertical Bifacial vs. Tilted Monofacial Photovoltaic Panels

Rehan Younas[a], Hassan Imran[a], Muhammad Hussnain Riaz[a],
Nauman Zafar Butt[a]

[a]*Department of Electrical Engineering, School of Science and Engineering, Lahore University of Management Sciences, Lahore 54792, Pakistan*

Abstract

An unprecedented demand for Food, Energy, and Water (FEW) resources over coming decades and the rising climate concerns require integrated FEW innovations with least environmental footprint. Collocating solar photovoltaic (PV) technology with agriculture is a promising approach towards dual land productivity that could locally fulfil growing food and energy demands particularly in rural areas. This 'agrivoltaic' (AV) solution can be highly suitable for hot and arid climates where an optimized solar panel coverage could prevent excessive thermal stress during harsh weather thereby increasing the crop yield and lowering the water budget. One of the concerns with using standard fixed tilt solar array structure that faces north/south (N/S) direction for AV farming is the spatial heterogeneity in the daily sunlight distribution for crops and soil water contents, both of which could affect crop yield. Dynamic tilt control through a tracking system can eliminate this problem but could increase the system cost and complexity. Here, we investigate east/west (E/W) faced vertical bifacial panel structure for AV farming and show that this could provide a much better spatial homogeneity for daily sunlight distribution relative to the fixed tilt N/S faced PV structure implying a better suitability for monoculture cropping. By modeling PV energy and crop yield under varying density (row to row pitch) for PV arrays and shade tolerances for crops, we show that E/W vertical bifacial panels can provide ∼5% better land productivity as compared to N/S faced fixed tilt panels for Lahore (31.5204° N, 74.3587° E) when PV array density is slightly lower than that of a standard solar farm. In contrast, when PV arrays are denser than the standard, land productivity for E/W vertical bifacial panels degrades due to mutual shading. These results, together with high inherent resilience to soiling (dust accumulation) losses for E/W vertical bifacial panels, indicate their attractive prospects for AV applications.

1

---

1. Introduction

Agrivoltaics (AV) is an emerging approach of harvesting energy and food together in a given land area that can maximize the land productivity with additional potential benefits including reduced irrigation budget, improved crop yield, agricultural land preservation, and, socio-economic welfare of farmers [1][2][3]. AV farming is rapidly attracting worldwide attention due to large scale spreading of solar photovoltaic energy systems which is prompting the need to develop effective solutions for its landscape integration that can minimize ecological changes to the land and favor local community [4][5]. In AV approach, photovoltaic (PV) panel arrays are designed to partially cover the crops with optimal density, elevation, and, tilt, which manipulate the desired balance for sharing sunlight intensity between energy and crop production. The PV covering could be leveraged to protect crop yield against adverse weather conditions, e.g., to minimize harmful thermal stress on plants in hot climate, and, to reduce leaching of soil due to excessive rain through water management [6][7]. Moreover, PV coverage has shown a lower water evaporation in the farm reducing the required water budget for irrigation by 20% [8]. Similarly, by sharing water for irrigation with cleaning of PV panels, operation cost for the system could be reduced. From socio-economic perspective, AV farming could make a significant improvement in the livelihood of farming communities and could accelerate solar energy investments to enable more sustainable economies.

Although the concept of collocating agriculture and photovoltaics was originally floated in 1982 by Goetzerberger [9], its large scale realization has only been seen within the past few years. The initial work by Goetzerberger presented an analytical model based on view factor approach and clear sky models and predicted that about two-thirds of the daily global radiation could be available to the crops in an AV farm at Freiburg (Latitude: 48°), Germany, having elevated solar panels with arrangement optimized for solar collection. Durpraz [6][10] predicted that 35 - 73% increase in land productivity was possible for Montpelier (Latitude 46.3°), France, when solar arrays were arranged at full and half densities that correspond to row to row pitch being twice and four times the height of the panels, respectively. These studies also introduced a metric called land equivalent ratio (*LER*), that was originally used for measuring efficacy of inter-cropping [3], to characterize the productivity of land for AV relative to the isolated solar energy

2

systems and agricultural farms. Predicted *LERs* for AV systems were remarkably high in the range of 1.3 to 1.6 [6][10]. Marrou [7] performed experiments on AV system in Montpelier (Latitude: 46.3°), France, for solar panel arrays at full and half densities and noted that minimal adaptations in the cropping practice were needed to switch from an open cropping to AV cropping. Cropping behavior was observed for both short cycle (lettuce, cucumber) and long cycle (durum wheat) crops. The study concluded that the main focus for developing AV system should be on exploring mitigation strategies for light reduction and optimal selection of crops [7].

Majumdar [4] modeled AV system at Pheonix Arizona and showed that south faced solar arrays titled at 30° received 60% and 80% of the total global radiation for half and quarter density of solar arrays respectively as compared to an open field. Malu [11] studied the AV potential for grape farming in Maharashtra (Latitude: 19.59°), India, and observed that it could increase the economic value of the land by 15 times as compared to the conventional farming. The study showed that a ground coverage of 26% with south tilted panel did not result into any loss in grape yield. Amaducci [12] showed that the reduction of global radiation under AV was more affected by panel density than by dynamic management of tilt through solar tracking. Sekiyama [13] did an experiment in Ichihara City (Latitude: 35.37°, Longitude: 140.13°), Japan, to study AV farming for corn. A comparison for the crop productivity was done for panel arrays at full vs. half density. It was found that the crop yield for the half density panels remarkably outperformed that of the open (control) farm by 5.6%.

Microclimatic benefits for the crops in an AV environment have also been demonstrated. Elamri [8] used simulation models to show that properly placed solar arrays could reduce the water requirement of the plants by 20% when 10% compromise in the crop yield or a slight increase in the crop cycle could be tolerated. Adeh [14] studied different microclimate parameters such as mean air temperature, relative humidity, wind speed and direction, and soil moisture for AV system in Oregon, USA. It was shown that the areas under PV solar panels resulted in a higher soil moisture, 90% more late season biomass, and, were 328% more water efficient.

Various studies reported so far on AV systems have used standard monofacial PV panel arrays that face N/S direction at a fixed or a dynamically controlled tilt. The potential for E/W faced bifacial solar panels has not yet been explored for AV, although the bifacial technology is attracting a great attraction in the commercial PV market due to its superior power conversion efficiency and rapidly decreasing panel prices. Besides the traditional N/S orientation, bifacial panels

could also be conveniently installed vertically facing East/West direction without any significant drop in the daily energy production [15]. The vertical tilt is in particular highly suitable for the environment which has high dust constituents since the dust has a low tendency to accumulate on a vertical surface. PV soiling (dust accumulation) losses are known to mitigate strongly as the panel tilt varies from horizontal to vertical [16]. Since solar panels in AV farm are expected to operate in a significantly dusty environment, especially during the tillage and harvesting seasons, vertical panels could be well suitable under these situations. It is however important to understand the trade-offs between the shading intensity/distribution and energy generation for a vertical E/W panel arrangement for AV application.

The purpose of this paper is to investigate the technological potential of E/W oriented vertical bifacial PV technology for AV and to compare its relative performance with respect to the fixed tilt N/S faced monofacial panel orientation. In particular, we address the following questions: (i) How does the daily cumulative radiation density that is available for crops vary for a given panel density? (ii) What is the relative uniformity/homogeneity of the shading patterns for the daily radiation received by the crops, (iii) How do the generated energy and crop yields for a given panel density vary for the two panel orientations? (iv) How does the land productivity, measured in terms of *LER*, vary as function of panel density and the crop's shade tolerance?, and, finally, (v) What is the effect of tilt angle (for N/S faced PV) on shade patterns and *LER*?

This paper is divided into four section. In Section 2 we describe the detailed methodology. Results are discussed in Section 3 whereas conclusions are furnished in Section 4.

2. Methodology

2.1. Calculation of Global Horizontal, Direct and Diffuse Irradiance

The global horizontal irradiance (I_{global}) at any location (latitude, longitude) on earth is characterized by irradiation intensity and position of the sun. Following a similar approach as reported in [15][17][18] for calculating I_{global}, we calculate the sun's trajectory *i.e.*, its temporal path for Lahore using NREL's algorithm [19] that is implemented in Sandia's photovoltaic modeling library (PVLib) [20]. The sun's trajectory is defined by its zenith (θ_z) and azimuth (γ_s) angles. θ_z is corrected for temperature and altitude effects in PVLib and γ_s is measured from north. Huarwitz clear sky model [21][22] was used to measure I_{global} with a one-minute time resolution. I_{global} calculated using PVLib was divided into direct and diffuse

components which are related as

$$I_{\text{global}} = I_{\text{dir}} \times \cos(\theta_{\text{z}}) + I_{\text{diff}} \qquad (1)$$

where I_{dir} and I_{diff} are direct normal and diffused horizontal irradiance respectively. We use Orgill and Hollands model [23] that computes diffuse fraction (DF) using sky clearness index (k_{T}) as

$$k_{\text{T}} = \frac{I_{\text{diff}}}{I_0 \times \cos(\theta_{\text{z}})} \qquad (2)$$

where I_0 is called the extra-terrestrial irradiance and can be computed analytically [24]. By computing k_{T} with a one-minute time resolution, I_{diff} was computed using Orgill and Hollands model and I_{dir} was computed using eq. (1) as

$$\left. \begin{array}{l} I_{\text{diff}} = DF \times I_{\text{global}} \\ I_{\text{dir}} = \frac{I_{\text{global}} - I_{\text{diff}}}{\cos(\theta_{\text{z}})} \end{array} \right\} \qquad (3)$$

2.2. Properties of Solar Farm and Energy Harvesting

The solar farm consists of solar modules of height (h) that are mounted at an elevation (E) above the ground. The modules are tilted at an angle β with respect to ground and the pitch (row-to-row separation) between them is p. For Lahore, Pakistan located in northern hemisphere, the modules are placed either in east-west faced or in south facing orientation. Throughout this paper, the east-west facing modules are considered bifacial and placed vertically, whereas the south facing modules are considered monofaical and tilted at some angle as shown in Fig. 1. The surface of the module facing the sky is taken as front surface whereas the other face is considered as back surface of the module, denoted by letters 'F' and 'B' respectively. The lower case letters 't' and 'b' represent the top and bottom points of the module respectively along the height of the module throughout this paper.

For calculating energy harvested by solar modules, we assume that arrays are long enough so that the edge effects are negligible. This allows for solving the problem in two-dimensions assuming symmetry in the third (infinitely long) dimension parallel to the row. The components of energy harvested through different types of irradiance are divided into four categories (*i.e.* direct, diffused, direct albedo and diffuse albedo irradiance) and will be discussed in detail in the coming section.

5

2.3. Direct Irradiance Collection

2.3.1. Calculation of Angle of Incidence

To compute the contribution of I_{dir} on the front (back) surface of the module, angle of incident (AOI) needs to be calculated. AOI is defined as the angle between the sun and the normal to the module surface as shown in Fig. 2. AOI for front surface of the module is given as [17]
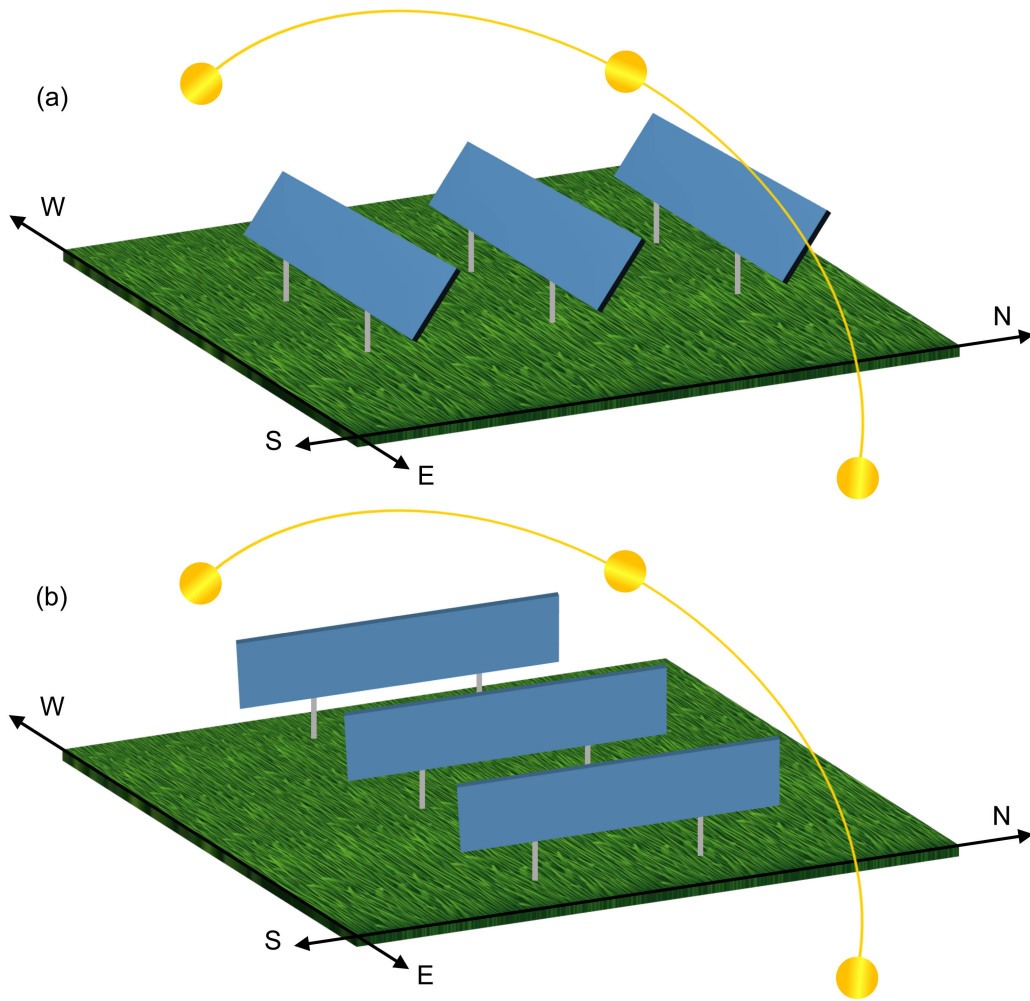

Figure 1: (a) Tilted monofacial south facing, and (b) vertical bifacial east-west facing solar modules.

$$\theta_F = \cos^{-1}\left(\cos\theta_z\cos\beta + \left[\sin\theta_z\sin\beta\cos\left\{(\gamma_M - 180) - (\gamma_s - 180)\right\}\right]\right) \quad (4)$$

where β is the tilt angle and γ_M is the azimuth angle of the module measured from north *i.e.* $\gamma_M = 90°$ for east-west facing modules and $\gamma_M = 180°$ for south facing modules. It is important to note that when $\theta_F > 90°$, it means that direct irradiance is now incident on the back surface of the module.

2.3.2. Calculation of Shadow Lengths

The shadow lengths cast by the direct beam of the sun on ground along the pitch or on the adjacent module are depicted in Fig. 2. For any given θ_F the lengths of the shadow cast by the top and bottom points of the module on the ground measured from $x = 0$ are denoted by $l_{s|t}$ and $l_{s|b}$ respectively (see Fig. 2) and given by

$$\left.\begin{array}{l} l_{s|t} = \frac{(E + h\cdot\sin\beta)\cdot\cos\theta_F}{\sin(90 - \beta + \theta_F)\cdot\sin\beta} \\[2mm] l_{s|b} = \frac{E\cdot\cos\theta_F}{\sin(90 - \beta + \theta_F)\cdot\sin\beta} \end{array}\right\} \quad (5)$$

The actual shadow length (l_s) on the ground is given by $l_s = l_{s|t} - l_{s|b}$. If $l_s > p$, then a part of the shadow will be cast on the adjacent module with height denoted by h_s (see Fig. 2) and given by
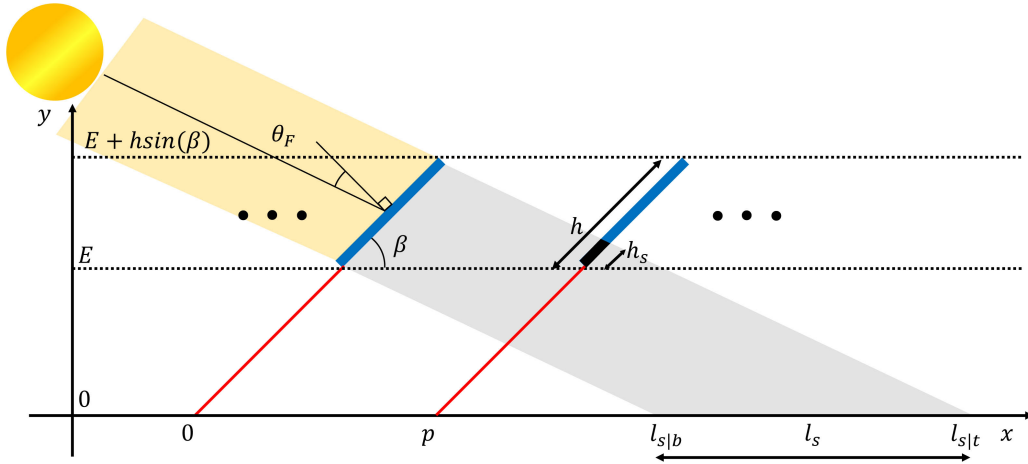

Figure 2: Illustration of direct sunlight incident on solar modules of height h, tilted at an angle β and mounted at an elevation E above the ground. The shadow length l_s on the ground and shadow height on the adjacent module h_s along with angle of incident θ_F are also depicted.

$$h_{\mathrm{s}} = \frac{\sin\left[90 + \theta_{\mathrm{F}} - \beta\right] \times \left[l_{\mathrm{s|t}} - p\right]}{\sin\left[90 - \theta_{\mathrm{F}}\right]} - \frac{E}{\sin(\beta)} \tag{6}$$

2.3.3. Energy Harvested from Direct Irradiance

Let's consider that the direct irradiance is incident on front surface of the module (*i.e.* $\theta_{\mathrm{F}} \leq 90°$) at any point z along the height of the module, then direct illumination components on unshaded part of the front module surface (*i.e.* $h > h_{\mathrm{s}}$) is $I_{\mathrm{dir}} \times \cos(\theta_{\mathrm{F}})$. The power generated by any point z on the front module surface for direct sunlight is given as

$$I_{\mathrm{M,dir|F}}(z) = \begin{cases} \left[1 - R(\theta_{\mathrm{F}})\right] \eta_{\mathrm{dir|F}} \times I_{\mathrm{dir}} \times \cos(\theta_{\mathrm{F}}) & ;\ z > h_{\mathrm{s}} \\ 0 & ;\ z \leq h_{\mathrm{s}} \end{cases} \tag{7}$$

where $R(\theta_{\mathrm{F}})$ is the angle dependent reflectivity of the module [25], and $\eta_{\mathrm{dir|F}}$ is the efficiency of the front surface of the module under direct light and considered equal to 19%. The back surface efficiency $\eta_{\mathrm{dir|B}}$ is supposed equal to $\eta_{\mathrm{dir|F}}$ for simplicity. Similarly, we compute $I_{\mathrm{M,dir|B}}$ for back surface of the module. The total power generated by direct irradiance per unit solar farm area is the sum of power generated by front and back surfaces of the module and given as

$$I_{\mathrm{M,dir}} = \frac{1}{p} \times \int_0^h \left[I_{\mathrm{M,dir|F}}(z) + I_{\mathrm{M,dir|B}}(z)\right] dz \tag{8}$$

2.4. Diffuse Irradiance Collection

2.4.1. Computation of Masking Angles and View Factors

We first determine the masking of diffused light on the module by the adjacent modules [15][17][18]. Let's consider a point z along the height of the module, the masking angles of diffuse light for front and back surfaces are denoted by $\psi_{\mathrm{sky|F}}$ and $\psi_{\mathrm{sky|B}}$ respectively as shown in Fig. 3 and given by

$$\left.\begin{aligned} \psi_{\mathrm{sky|F}}(z) &= \tan^{-1}\left[\frac{h - z \cdot \sin\beta}{p - (h-z)\cos\beta}\right] \\ \psi_{\mathrm{sky|B}}(z) &= \tan^{-1}\left[\frac{h - z \cdot \sin\beta}{p + (h-z)\cos\beta}\right] \end{aligned}\right\} \tag{9}$$

The view factor of any point z on the module towards the sky for front and back surfaces are denoted by $F_{\mathrm{d}z \to \mathrm{sky|F}}$ and $F_{\mathrm{d}z \to \mathrm{sky|B}}$ and are given by [26]
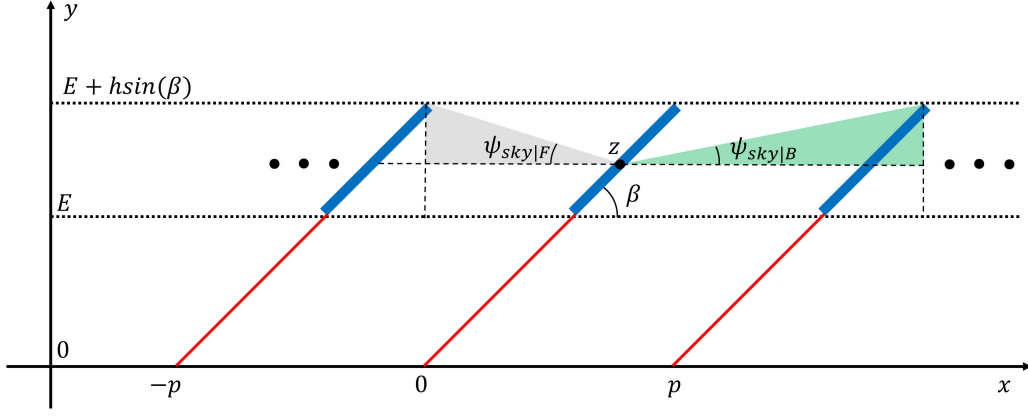
Figure 3: Masking of diffuse light on the face of the module by the adjacent modules on either side.

$$
\left.
\begin{aligned}
F_{\text{d}z\to\text{sky}|\text{F}}(z) &= \tfrac{1}{2}\left[1 - \sin\{\psi_{\text{sky}|\text{F}}(z)\}\right] \\
F_{\text{d}z\to\text{sky}|\text{B}}(z) &= \tfrac{1}{2}\left[1 - \sin\{\psi_{\text{sky}|\text{B}}(z)\}\right]
\end{aligned}
\right\}
\tag{10}
$$

2.4.2. Energy Harvested From Diffuse Irradiance

The power generated by any point z on the module for diffuse irradiance for both front and back surfaces is given by

$$
\left.
\begin{aligned}
I_{\text{M,diff}|\text{F}}(z) &= \eta_{\text{diff}|\text{F}}\left(I_{\text{diff}} \times F_{\text{d}z\to\text{sky}|\text{F}}\right) = \eta_{\text{diff}|\text{F}}\left(I_{\text{diff}} \times \tfrac{1}{2}\left[1 - \sin\{\psi_{\text{sky}|\text{F}}\}\right]\right) \\
I_{\text{M,diff}|\text{B}}(z) &= \eta_{\text{diff}|\text{B}}\left(I_{\text{diff}} \times F_{\text{d}z\to\text{sky}|\text{B}}\right) = \eta_{\text{diff}|\text{B}}\left(I_{\text{diff}} \times \tfrac{1}{2}\left[1 - \sin\{\psi_{\text{sky}|\text{B}}\}\right]\right)
\end{aligned}
\right\}
\tag{11}
$$

where $\eta_{\text{diff}|\text{F}}$ and $\eta_{\text{diff}|\text{B}}$ are the efficiencies of front and back surfaces of the module respectively for diffused light and assumed equal to $\sim 16\%$. The total power generated by diffuse irradiance per unit solar farm area is the sum of power generated by front and back surfaces of the module and given as

$$
I_{\text{M,diff}} = \frac{1}{p} \times \int_0^h \left[I_{\text{M,diff}|\text{F}}(z) + I_{\text{M,diff}|\text{B}}(z)\right] dz
\tag{12}
$$

9

2.5. Direct Albedo Collection

2.5.1. Computation of Masking Angles and View Factors

Let's consider a time during the day when $\theta_F \leq 90°$ and a shadow of length l_s on the ground. To compute the contribution of direct albedo at any point z on the module, the angles subtended by the edges of the shadow (*i.e.* $l_{s|t}$ and $l_{s|b}$ are computed for both front and back surfaces of the module as shown in Fig. 4.

Let the angles at the front and back faces of the module at any point z subtended from right and left edges of the shadow in the ith pitch be $\psi_{t|F}^{(i)}$ and $\psi_{b|F}^{(i)}$ and $\psi_{t|B}^{(i)}$ and $\psi_{b|B}^{(i)}$ respectively (see Fig. 4), and given by

$$
\left.
\begin{aligned}
\psi_{t|F}^{(i)}(z) &= \tan^{-1}\left[\frac{E+z\cdot\sin\beta}{i\times p-l_{s|t}+\frac{E+z\cdot\sin\beta}{\tan\beta}}\right] \\
\psi_{b|F}^{(i)}(z) &= \tan^{-1}\left[\frac{E+z\cdot\sin\beta}{i\times p-l_{s|b}+\frac{E+z\cdot\sin\beta}{\tan\beta}}\right] \\
\psi_{t|B}^{(i)}(z) &= 180° - \tan^{-1}\left[\frac{E+z\cdot\sin\beta}{-(i-1)\times p-l_{s|t}+\frac{E+z\cdot\sin\beta}{\tan\beta}}\right] \\
\psi_{b|B}^{(i)}(z) &= 180° - \tan^{-1}\left[\frac{E+z\cdot\sin\beta}{-(i-1)\times p-l_{s|b}+\frac{E+z\cdot\sin\beta}{\tan\beta}}\right]
\end{aligned}
\right\}
\tag{13}
$$

The view factors for front surface of the module from point z to the unshaded part of the ground can now be given as

$$
F_{dz\rightarrow Ugnd|F}(z) = \frac{1}{2}\times
\begin{cases}
\sin\beta - \sin\left(\psi_{t|F}^{(i)}\right) + \sum_i\left\{\sin\left(\psi_{b|F}^{(i)}-\psi_{t|F}^{(i+1)}\right)\right\} & ; \theta_F \leq 90° \\
\sin\beta - \sin\left(\psi_{b|F}^{(i)}\right) + \sum_i\left\{\sin\left(\psi_{t|F}^{(i)}-\psi_{b|F}^{(i+1)}\right)\right\} & ; \theta_F > 90°
\end{cases}
\tag{14}
$$

Similarly for the back surface, $F_{dz\rightarrow Ugnd|B}$ can also be computed based upon eq. (14).

2.5.2. Energy Harvested From Direct Albedo Irradiance

In order to compute the direct albedo collected at the module, the direct irradiance reaching the unshaded part of the ground at any given time needs to be computed and given by

$$
I_{gnd;dir} = I_{dir} \times \cos(\theta_z)
\tag{15}
$$

The power received by at any point z on the front and back faces of module due to direct albedo is given by

$$
\left.
\begin{aligned}
I_{M,Alb:dir|F}(z) &= I_{gnd;dir} \times \eta_{diff|F} \times R_A \times F_{dz\rightarrow Ugnd|F}(z) \\
I_{M,Alb:dir|B}(z) &= I_{gnd;dir} \times \eta_{diff|B} \times R_A \times F_{dz\rightarrow Ugnd|B}(z)
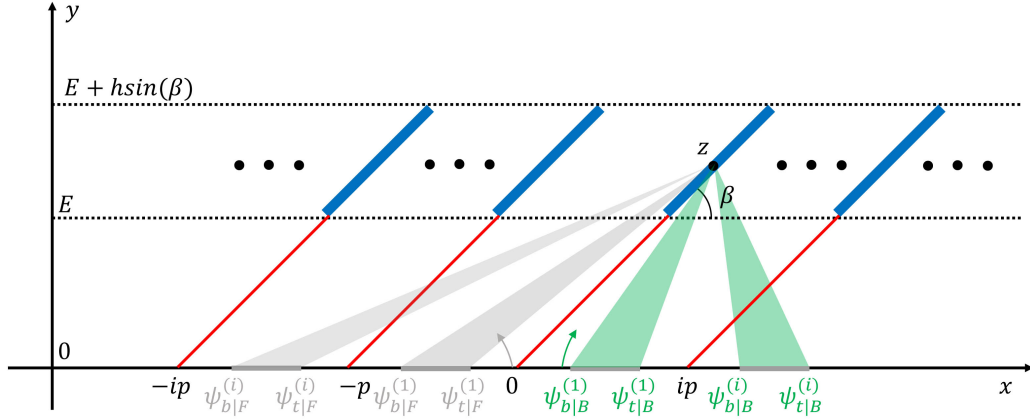\end{aligned}
\right\}
\tag{16}
$$

Figure 4: The angles subtended by the edges of the shade on the ground due to direct irradiance at a given time on the front and back surfaces of the modules. The green and gray arrow represent that angles are measured from the ground in clockwise and anti-clockwise direction respectively.

where R_A is the ground albedo and considered equal to 0.25 in all calculations. The total power generated by direct albedo per unit solar farm area is given as

$$I_{\text{M,Alb:dir}} = \frac{1}{p} \times \int_0^h \left[I_{\text{M,Alb:dir|F}}(z) + I_{\text{M,Alb:dir|B}}(z) \right] dz \tag{17}$$
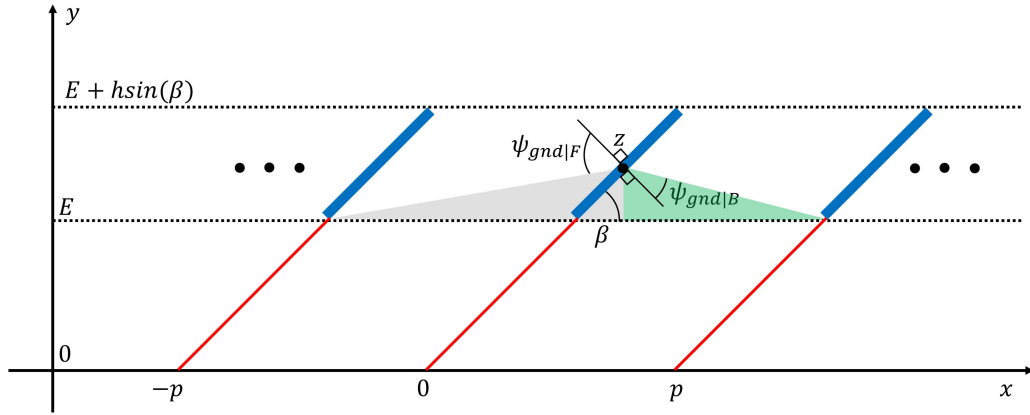
Figure 5: Masking of diffuse albedo light on the face of the module by the adjacent modules in either direction.

11

2.6. Diffuse Albedo Collection

2.6.1. Computation of Masking Angles and View Factors

In order to compute the contribution of diffuse albedo, the masking angles towards the ground by adjacent panels need to calculated for any point z on the panel. Let's consider that $\psi_{\text{gnd}|F}$ and $\psi_{\text{gnd}|B}$ be the masking angles for the front and back surfaces of the module as shown in Fig. 5 and can be computed for any given value of z as [17]

$$\left.\begin{array}{l} \psi_{\text{gnd}|F}(z) = \left|90 - \beta - \tan^{-1}\left[\frac{z \cdot \sin\beta}{p + z \cdot \cos\beta}\right]\right| \\[2mm] \psi_{\text{gnd}|B}(z) = \left|90 - \beta - \tan^{-1}\left[\frac{z \cdot \sin\beta}{p - z \cdot \cos\beta}\right]\right| \end{array}\right\} \tag{18}$$

The view factor of any point z on the module towards the ground for both front and back surfaces are denoted by $F_{\text{d}z \to \text{gnd}|F}(z)$ and $F_{\text{d}z \to \text{gnd}|B}(z)$ and are given by

$$\left.\begin{array}{l} F_{\text{d}z \to \text{gnd}|F}(z) = \frac{1}{2}\left[1 - \psi_{\text{gnd}|F}(z)\right] \\[2mm] F_{\text{d}z \to \text{gnd}|B}(z) = \frac{1}{2}\left[1 - \psi_{\text{gnd}|B}(z)\right] \end{array}\right\} \tag{19}$$

2.6.2. Energy Harvested From Diffuse Irradiance

The power generated by diffuse albedo for any point z by the front and back surfaces of the module is then given by

$$\left.\begin{array}{l} I_{\text{M,Alb:diff}|F}(z) = \eta_{\text{diff}|F} \times I_{\text{diff}} \times R_A \times F_{\text{d}z \to \text{gnd}|F}(z) \\[2mm] I_{\text{M,Alb:diff}|B}(z) = \eta_{\text{diff}|B} \times I_{\text{diff}} \times R_A \times F_{\text{d}z \to \text{gnd}|B}(z) \end{array}\right\} \tag{20}$$

Here, we have assumed that masking of diffuse light reaching the ground is negligible. This may have a minor effect on the quantitative energy calculations but the effect is expected to be similar for both N/S and E/W faced panels.

$$I_{\text{M,Alb:diff}} = \frac{1}{p} \times \int_0^h \left[I_{\text{M,Alb:diff}|F}(z) + I_{\text{M,Alb:diff}|B}(z)\right] dz \tag{21}$$

2.7. Direct Light Shadowing for Finite Farm Area

A two-dimensional model for spatial shade distribution is developed to better understand the edge effects due to direct light obstruction from panels. To calculate the amount of direct light shadowing at any observation point (OP) due to the panels, we assimilate the panels as polygons with four edges defined through their cartesian coordinates (x_e, y_e, z_e). The coordinates of observation points (x_{op}, y_{op}, z_{op})
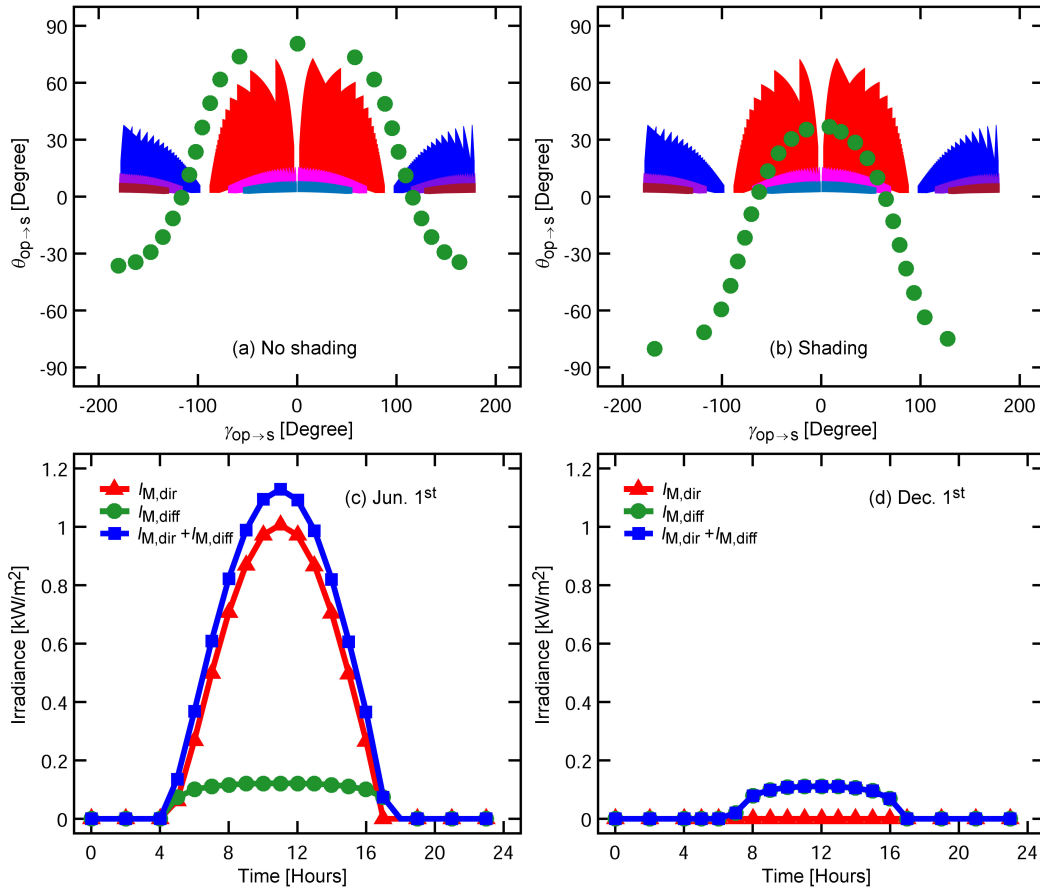
Figure 6: Sun path (green symbols) during a day and solar coordinates of south faced monofacial tilted PV modules as seen from an observation point (OP) at 1.5 m height, above the ground level, located along ($x = 27$ m, $y = 31$ m). This is a test point which lies in the open region of the AV farm. (a) Plotted is a scenario where op does not come under module's shadow any time during the day. (b) Situation where OP is always under shadow. (c,d) Solar radiation received at the considered OP. When the op does not come under module's shadow (June 1st), it receives both the direct as well as the diffused sunlight. When the OP is under module's shadow (Dec. 1st), it receives only the diffused sunlight.

as well as for the panels were calculated with reference to an arbitrary point of origin located at north-east corner of the farm.The solar coordinates for a given OP with respect to a panel are then calculated in terms of elevation ($\theta_{\mathrm{op}\rightarrow s}$) and azimuth ($\psi_{\mathrm{op}\rightarrow s}$) angles using [27]
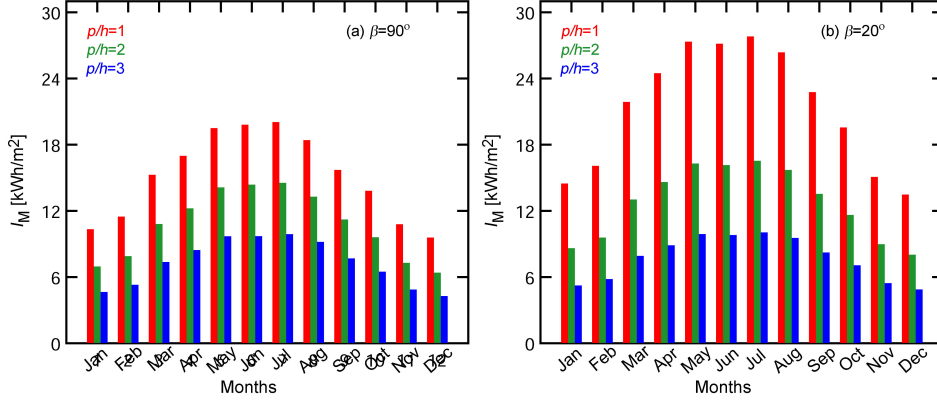
Figure 7: Power generated in (a) E/W PV, and (b) N/S PV farm tilted at $\beta = 20°$ during all months of the year for different values of panel density.

$$\theta_{\text{op} \rightarrow \text{s}} = \sin^{-1} \left[\frac{z_{\text{e}} - z_{\text{op}}}{\sqrt{(x_{\text{e}} - x_{\text{op}})^2 + (y_{\text{e}} - y_{\text{op}})^2 + (z_{\text{e}} - z_{\text{op}})^2}} \right] \tag{22}$$

and

$$\psi_{\text{op} \rightarrow \text{s}} = \cos^{-1} \left[\frac{y_{\text{e}} - y_{\text{op}}}{\sqrt{(x_{\text{e}} - x_{\text{op}})^2 + (y_{\text{e}} - y_{\text{op}})^2}} \right] \tag{23}$$

$\theta_{\text{op} \rightarrow \text{s}}$ and $\psi_{\text{op} \rightarrow \text{s}}$ for all solar panels in the farm were calculated and were compared with corresponding angles for the sun. This was used to find whether there is any obstruction to the direct path from the sun to the OP due to panels as shown in Fig. 6. At any given time, if the solar coordinates lie inside the region bounded by $\theta_{\text{op} \rightarrow \text{s}}$ and $\psi_{\text{op} \rightarrow \text{s}}$, the OP was considered to be under shade hence receiving the diffused light only, for which $I_{\text{op}} = I_{\text{diff}}$. Otherwise, the OP was considered to be receiving both direct as well as diffused sunlight ($I_{\text{op}} = I_{\text{gnd;dir}} + I_{\text{diff}}$). The cumulative radiation incident at a specific crop height was calculated as the percentage ratio of light received under panel coverge to the total incident light with no panels installed

$$G_{\text{GR}} = \frac{1}{k} \sum_{\text{op}=1}^{k} \frac{I_{\text{op}}}{I_{\text{global}}} \times 100\% \tag{24}$$
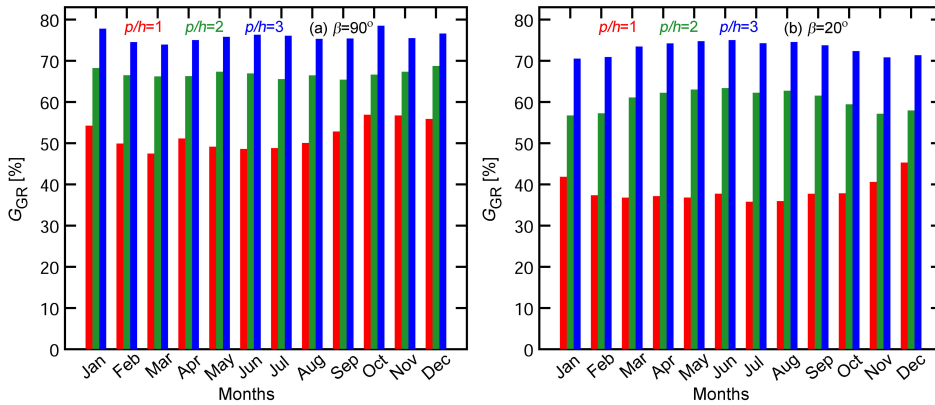
Here, k is varied to cover the entire farm area.

14

Figure 8: G_{GR} for (a) E/W PV, and (b) N/S PV farm tilted at $\beta = 20°$ during all months of the year for different values of panel density.

2.8. Land Equivalent Ratio

To quantify the performance of AV farm, land equivalent ratio (*LER*) is a commonly used metric in the literature [6]. It encapsulates the land productivity for the energy system and the crop output for AV farm relative to that for the standalone energy and crop systems using the same land. *LER* is given by the follow-
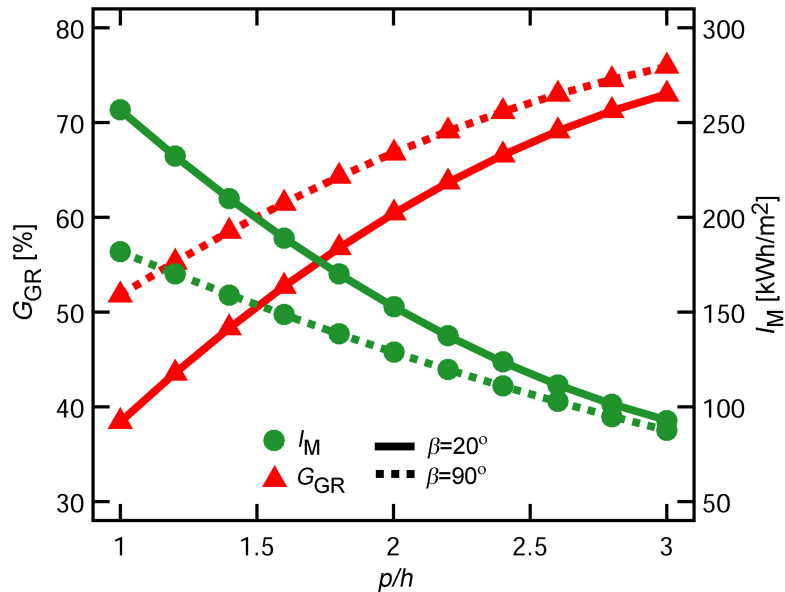

Figure 9: G_{GR} and I_M as a function of *p/h* for E/W and N/S PV configurations.

15

ing relationship

$$LER = \frac{Y_c(AV)}{Y_c(OF)} + \frac{Y_e(AV)}{Y_e(PV)} \tag{25}$$

where

$Y_c(AV)$ = Crop yield for AV farm

$Y_c(OF)$ = Crop yield for open farm with no PV panels installed

$Y_e(AV)$ = Energy yield for AV farm

$Y_e(PV)$ = Energy yield for traditional solar PV farm

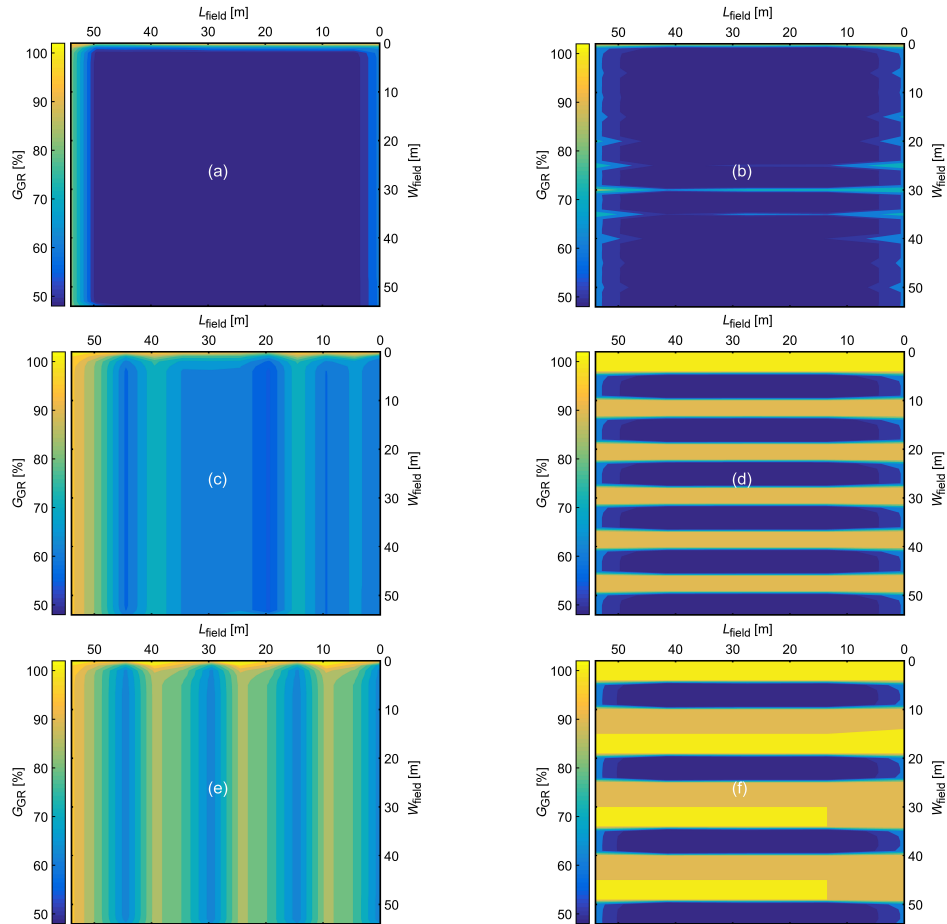For calculating $Y_c(AV)$, we assume that panels are ground mounted ($E = 0$) at

Figure 10: Contour maps of E/W PV (a,c,e) and N/S PV farm (b,d,f) configurations for the month of June and for three different values of panel density (p/h = 1, 2, 3 respectively.)

$p/h \approx 2$, while the tilt is kept at 20° and 90° for N/S and E/W faced panels respectively. Crop yield can vary under the local climate of an AV farm as compared to an open farm. The specific response for a crop yield in an AV farm may depend on many factors including the sensitivity of the crop to the temporal/spatial intensity of shade, weather conditions, microclimate factors, irrigation/rain amounts *etc.* Marrou [7] showed that among various factors, the effect of the intensity of radiation is the most dominant for crops grown in an AV farm. In our model, we therefore assume that the crop yield is primarily affected by the intensity of shade caused by solar panels. For the behavior of crop yield as a function of sunlight, we assume a linear relation between crop yield and the shade intensity. This may not apply in general to every crop but could be a good approximation for a set of crops. For example, Durpraz [6] showed that the yield vs. photosynthetically active radiation (PAR) for durum wheat in an AV farm had a good correlation to a linear fit for a broad range of PAR at various panel densities. The yield ratio for crop in AV farm could then be written as

$$\frac{Y_c(\text{AV})}{Y_c(\text{OF})} = m \times G_{\text{GR}} + (1 - m) \tag{26}$$

where the linear slope (m) is kept variable as an indicator for the crop sensitivity to the shade. A smaller m represents that crop yield is more tolerant to shade.

3. Results and Discussion

The performance of agrivoltaic system has been assessed for two different panel orientations: (i) North/South (N/S) faced fixed tilt monofacial panels (N/S PV), and, (ii) East/West (E/W) faced vertical bifacial panels (E/W PV) for Lahore (31.5204° N, 74.3587° E). The energy production and crop yield have been computed as a function of variation in panel density and tilt angle (for N/S PV) for a set of crop sensitivities to the shade. The farm area is kept constant at 55×55 m^2 for both panel orientations to calculate G_{GR} including the edge effects. Three cases for panel density are considered: standard panel density ($p/h \approx 2$), high panel density ($p/h \approx 1$), and, low panel density ($p/h \approx 3$). For each case, p is varied without changing h.

3.1. Effect of Pitch

Fig. 7 presents a comparison between the monthly energy production for N/S PV at fixed tilt of 20° and E/W PV for varying panel density. As expected, the energy production during summer months are higher for both panel orientations

that corresponds to the longer sunshine hours and higher elevation angles of sun during summer. At low panel density, E/W PV shows a similar energy yield as that of N/S PV. As panel density is increased, N/S PV shows a relatively higher energy output. This is due to the fact that for higher panel densities, mutual shading between the adjacent rows of panels gets much more significant for E/W PV which
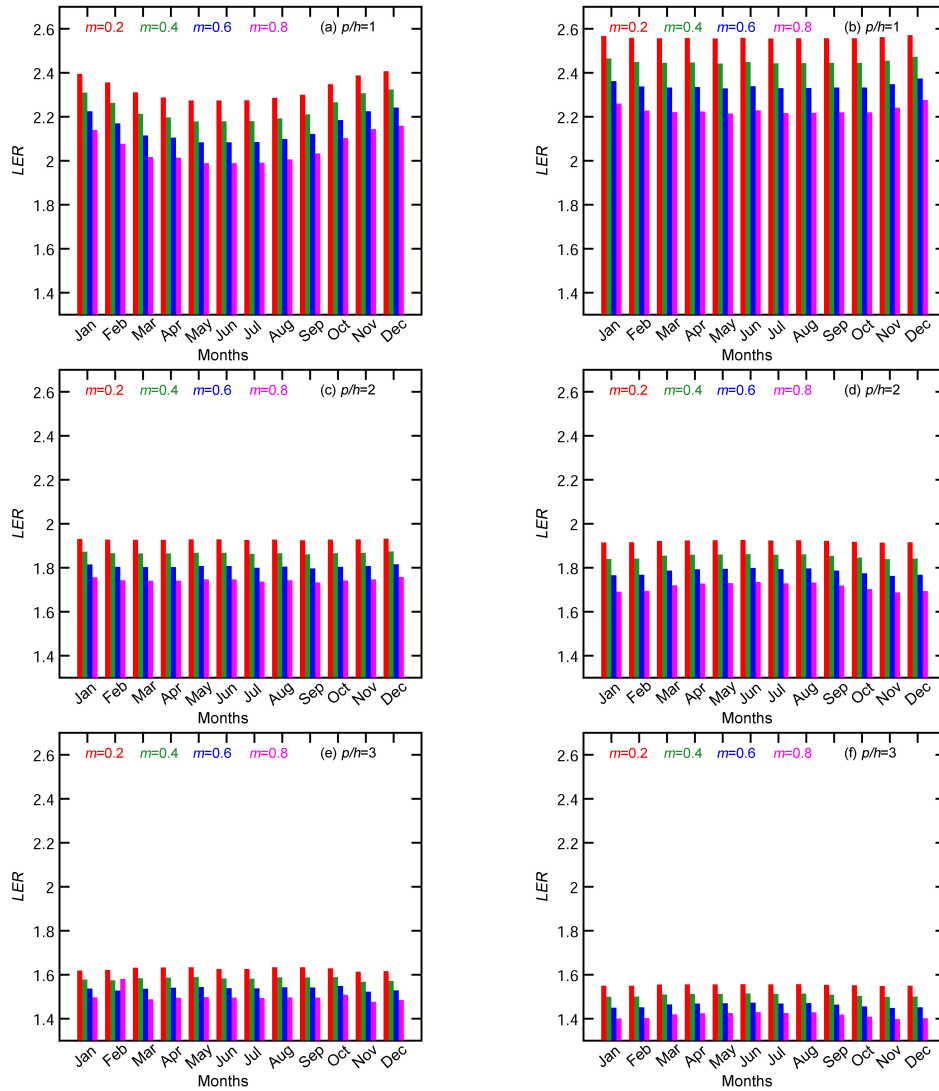

Figure 11: Land equivalent ratio (*LER*) for E/W PV farm for (a) *p/h* = 1 , (c) *p/h* = 2 and (e) *p/h* = 3 and *LER* for N/S PV farm for (b) *p/h* = 1 , (d) *p/h* = 2 and (f) *p/h* = 3 respectively for different values of *m*.

reduces its energy output as compared to that for N/S PV.

Fig. 8 shows monthly variation in G_{GR} at different panel densities for the two panel orientations. E/W PV provides a relatively higher G_{GR} in general for all panel densities. This trend becomes more significant for winter months and for high panel density. Interestingly, high density of panels in E/W PV also shows reduced energy output due to mutual shading (Fig. 7). This highlights the fact that PV mutual shading inversely affects the energy production and sunlight received by the crops.

Fig. 9 summarizes the annual energy production and G_{GR} for both panel orientations. For low density of panels, mutual shading between panels is not so significant, the energy production for E/W PV and N/S PV is similar while the annual G_{GR} is 76% and 73% respectively. For standard panel density, the energy production for E/W PV drops by $\sim$16% relative to N/S PV whereas its relative G_{GR} increases by 11%. For high density panels, there is about 29% drop in relative energy production for E/W PV while the relative G_{GR} is 35% higher. These trends illustrate a trade-off between G_{GR} vs. energy as the panel density increases from $p/h = 3$ to $p/h = 1$.

3.1.1. Spatial Light Distribution (Homogeneity) Across Farm

To get an insight into the light distribution for the crops, we plot the monthly cumulative G_{GR} distribution across the farm area at the height of 1.5m above ground for both panel orientations during the month of June at different panel densities in Fig. 10. For N/S PV at standard and low panel density, the spatial distribution for direct light shows a pattern of high contrast depicted by sharp transitions between regions of high/low shading. This pattern arises for N/S PV because the spatial regions directly below the panels receive a significantly lower light as compared to those between two adjacent rows of panels resulting into G_{GR} of $< 30\%$ and $> 90\%$ respectively. This high spatial heterogeneity for G_{GR} suggests that the cropping practice for N/S PV may also be adjusted accordingly. For example, a polyculture may be beneficial for N/S PV in which regions of high G_{GR} could be allocated for the crops having a high light requirement, whereas, crops that are more shade tolerant could be grown in rows where G_{GR} is smaller. In contrast, for E/W PV, the G_{GR} across the farm is much more homogeneous. No abrupt contrast could be seen for G_{GR} which varies across a much smaller range across the farm. This suggests that E/W PV might be more suitable for mono-crop farming that has a uniform light requirement across the farm. For high panel density, light distribution for crops across the farm becomes largely homogeneous (except at the edges) for both panel orientations. This is because the pitch is now

19

so small that there is essentially no spatial region where the shading caused by the panels is insignificant even for the case of N/S PV.

3.1.2. Land Equivalent Ratio

Fig. 11 presents a comparison between the monthly land equivalent ratios (*LER*) for E/W vs. N/S PV for varying shade tolerance levels for crops at different panel densities. The sensitivity to the shade for the crop is parametrized through the variable *m* (as defined in equation (26)) where a bigger *m* implies a higher sensitivity to the shade. For low panel density, E/W PV has a relatively better *LER* while the trend becomes flipped for the case of high panel density. For standard panel density, E/W PV shows a slightly better *LER* which is more prominent for crops which are less shade tolerant. The annual *LER* for both panel orientations are summarized in Table 1. For all panel densities, a lower crop sensitivity to the shade results in a higher *LER* while the monthly variations in *LER* are not as significant. The energy and crop yields (as defined in equation (25)) for AV normalized to that for standalone energy and crop systems respectively are shown in Fig. 12 for E/W and N/S PV as a function of the panel density. An inverse trend could be observed for energy and crop yields as the panel density is varied. The former shows a relative improvement while the latter shows degradation as panel density is increased. While the crop yield for E/W PV always exceeds as compared to that for N/S PV for all panel densities, the energy yield for N/S PV is higher for the case of high panel density. Moreover, the difference between the crop yield for the two panel orientations widens for the crops which are more sensitive to the shade and becomes negligible when panel density is low.

3.2. Effect of Tilt Angle

For N/S PV at locations in the northern hemisphere, the PV tilt angle optimized for energy yield is known to decrease from winter to summer months [16][28][29]. For AV systems, the optimal tilt angle has to be adjusted according to the desired trade-off between sunlight sharing between panels and crops. Fig. 13 shows the monthly energy yield and G_{GR} for N/S PV with tilt angle varying between 20° to 60°. During summer season, energy output of panels placed at 20° tilt angle is significantly higher than that placed at higher tilts while the corresponding G_{GR} is lower. The trend flips during winter season although the quantitative shift in energy and G_{GR} is much more pronounced in summer as compared to winter.

Fig. 8 shows spatial distribution for G_{GR} across the farm area for N/S PV with varying tilt angle for the months of June (Fig. 14(a,b,c)) and December
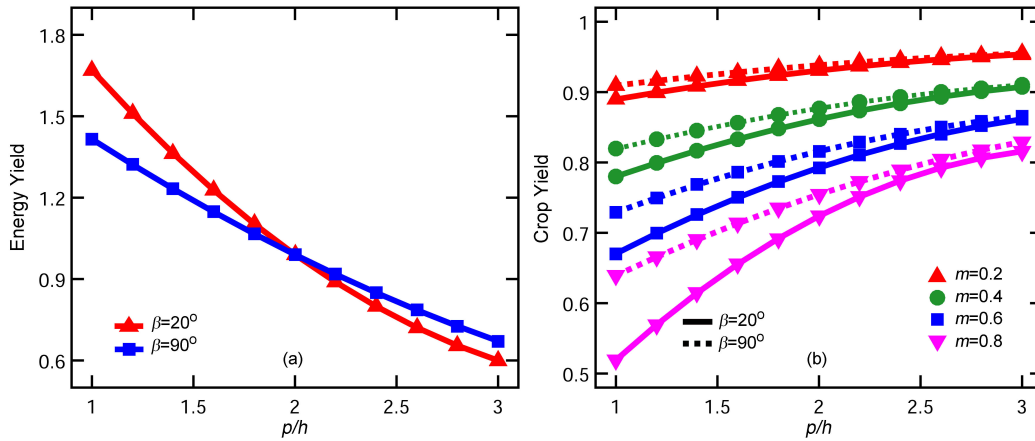
20

Figure 12: (a) Energy and (b) Crop yield as a function of *p/h* for E/W and N/S PV configurations.
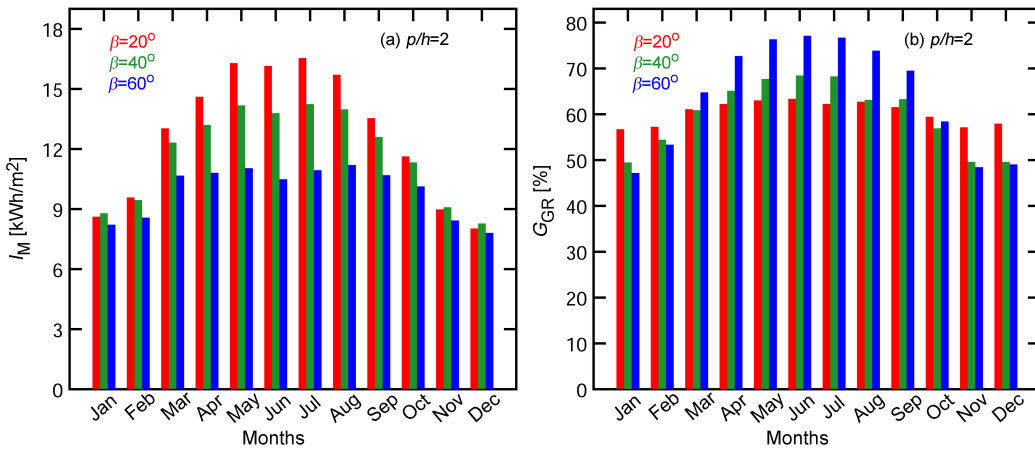

Figure 13: Effect of tilt angle on (a) I_M and (b) G_{GR} values in N/S PV configuration for all months of the year .

(Fig. 14(d,e,f)). During summer, an increase in tilt angle results in widening of the spatial region that receives a high G_{GR} (> 90%) as shown in Fig. 14(a,b,c). In contrast, for December, increasing tilt angle results in a relative squeezing of the region that receives high G_{GR}. The relative change in G_{GR} is however not as significant for December as compared to that for June.

Fig. 15 presents monthly *LER* for various tilt angles for N/S PV. For $\beta = 20°$, *LER* is relatively high and the monthly variation in *LER* are not significant. For higher β summer months show a significant drop in *LER* that is related to the drop in PV energy generation as shown in Fig. 13(a). The crop yield is relatively less

Table 1: Summary of *LER* values for E/W and N/S PV configurations at different panel densities and shade tolerance levels.

			m=0.2	*m*=0.4	*m*=0.6	*m*=0.8
	$p/h=1$	$\beta = 20°$ [N/S]	2.56	2.45	2.34	2.23
		$\beta = 90°$ [E/W]	2.33	2.24	2.14	2.05
LER	$p/h=2$	$\beta = 20°$ [N/S]	1.92	1.85	1.78	1.71
		$\beta = 90°$ [E/W]	1.93	1.87	1.81	1.74
	$p/h=3$	$\beta = 20°$ [N/S]	1.55	1.51	1.46	1.42
		$\beta = 90°$ [E/W]	1.63	1.58	1.54	1.50

Table 2: Summary of *LER* values for different tilt angles in a N/S PV farm for different crop shade tolerance levels.

		m=0.2	*m*=0.4	*m*=0.6	*m*=0.8
	$\beta = 20°$ [N/S]	1.92	1.85	1.78	1.71
LER	$\beta = 40°$ [N/S]	1.86	1.79	1.72	1.65
	$\beta = 60°$ [N/S]	1.74	1.67	1.61	1.55

affected by the change in β as shown in Fig. 16. *LER* for various β are summarized in Table 2.

4. Summary and Conclusions

In this study, we have compared the relative effectiveness of vertical bifacial E/W facing panels vs. standard fixed tilt N/S facing monofacial panels for agrivoltaic systems. We used Sandia photovoltaic modeling library (PVLib) for calculating Sun's trajectory and irradiation intensity. A new model to calculate energy yield including albedo collection and ground shading for the elevated panels has been developed. The shade distributions including the edge effects for the crops are modeled by implementing analytical functions related to panels' geometry and placement relative to Sun's trajectory in MATLAB. We conclude that:

- Vertical E/W bifacial PV can increase land productivity by ∼5% relative to that of the fixed tilt N/S PV for panel density (p/h = 3) which is slightly
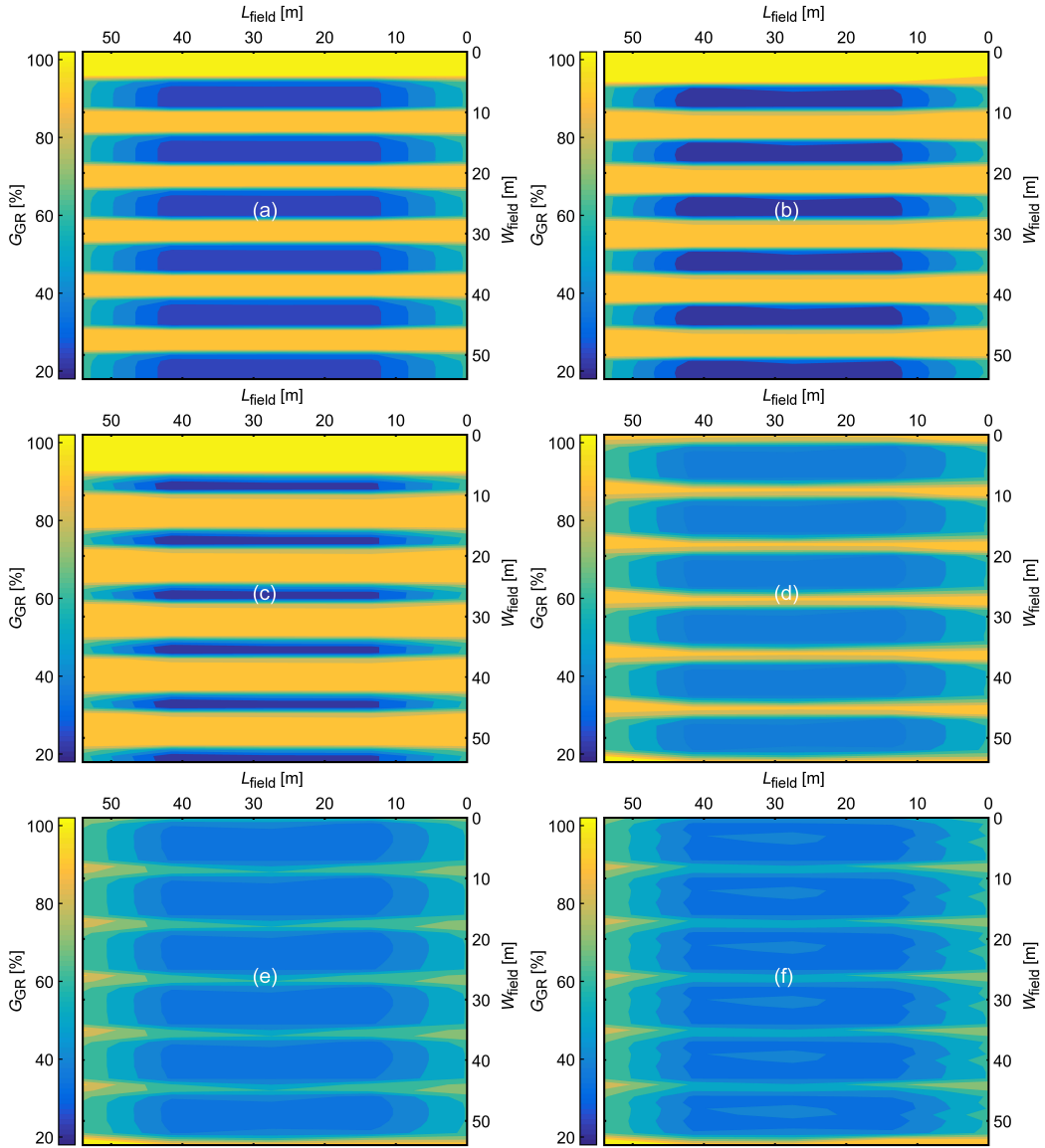

Figure 14: Contour maps for a N/S PV farm having *p/h* = 1. Maps show a variation in light homogeneity as a function of panels' tilt angle. While an increase in tilt angle during summer time (a,b,c) results in a high contrast in light distribution, it is nearly unchanged during winter season (d,e,f).
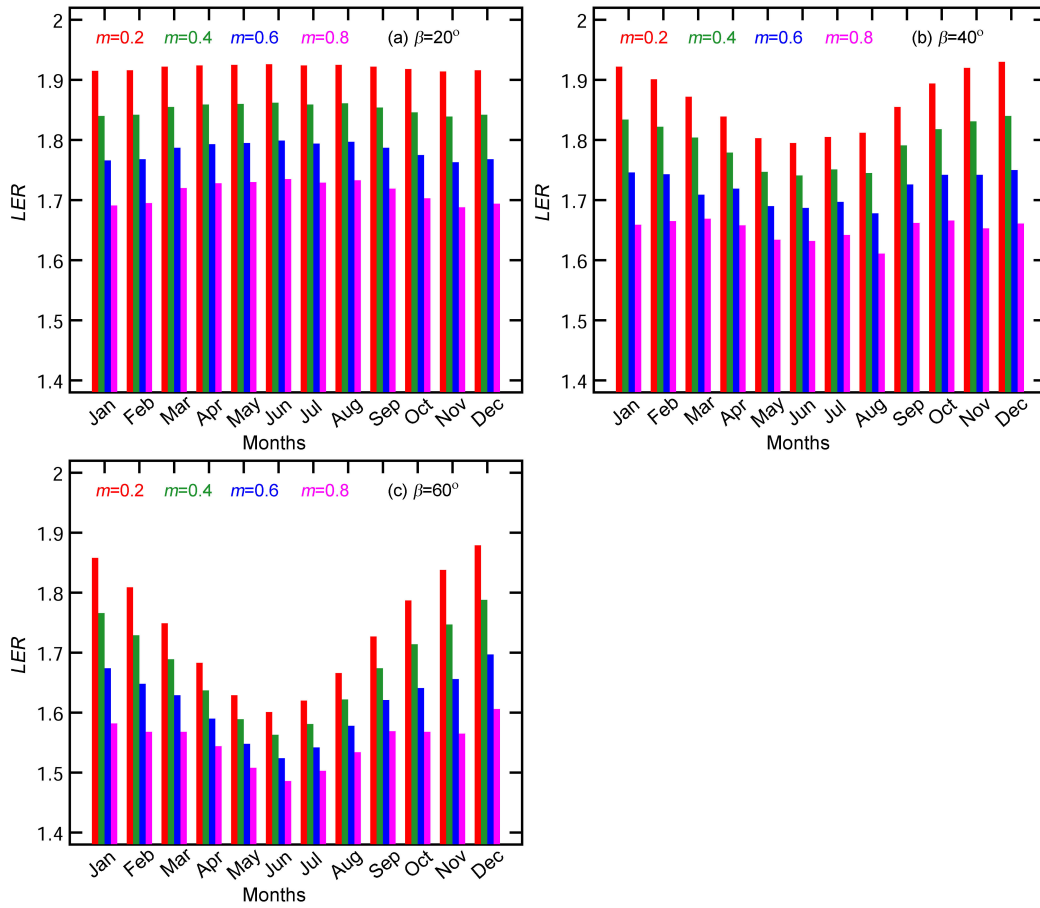
Figure 15: *LER* values at different tilt angles for N/S PV farms.

lower than that used in standard (p/h = 2) solar farms. This is primarily due to an overall lower daily shading intensity below the panels for E/W PV with similar energy production relative to N/S PV.

- The spatial distribution for sunlight intensity over the crops in vertical E/W PV is much more homogeneous as compared to tilted N/S PV for standard and lower panel density. The N/S PV shows shade patterns of high contrast corresponding the spatial regions vertically below the panels and those which are under the sun between the adjacent rows of panels. The spatial distribution for N/S PV becomes much more homogeneous for high panel density ($p/h = 1$).
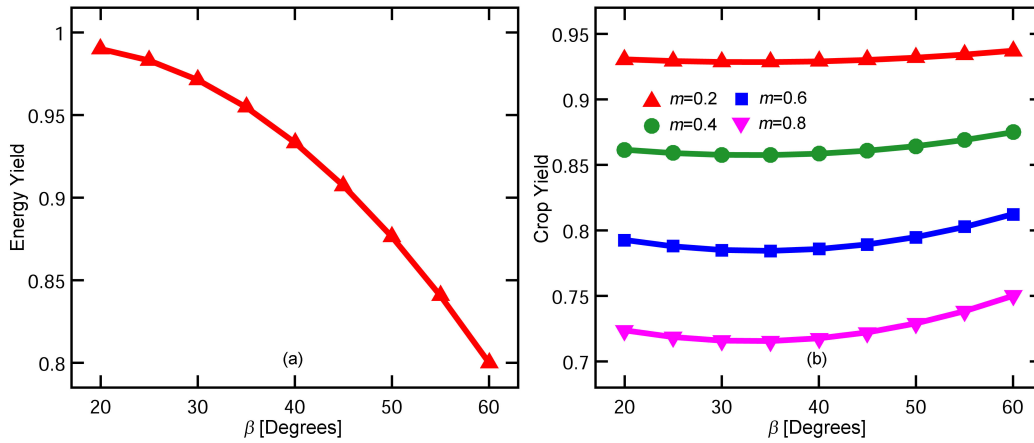
Figure 16: (a) Energy and (b) Crop yield as a function of tilt angle.

- For panel arrays that have higher density ($p/h = 1$), N/S fixed tilt PV provide $\sim$8% better land productivity as compared to that for E/W PV. Moreover, at this density, both panel orientations show spatial homogeneity for the sunlight received by the crops. The crop yield is still relatively better for E/W PV but its energy yield significantly drops due to mutual shading between panels.

- For both E/W and N/S PV orientations at any given panel density, *LER* drops when the crop's tolerance to shade decreases. For standard panel density, lesser ($m = 0.8$) shade tolerant crops drop *LER* by 11% as compared to higher ($m = 0.2$) shade tolerant crops.

- The impact of crop's shade tolerance on *LER* increases as the panel density in the farm is increased. For the highest panel density ($p/h = 1$) considered in this work, *LER* increases by 15% when crop shade tolerance is increased (from $m = 0.8$ to $m = 0.2$). For the same change in *m* for less dense ($p/h = 3$) panels, *LER* increases by 9%.

- For N/S PV, increasing tilt angle above an optimal value results in an increased variation in the monthly values for *LER*. Moreover, tilt angles that are higher than the optimal reduce the annual *LER*.

- The best cropping practices for E/W vs. N/S PV configurations may be very different. For N/S PV, a polyculture looks suitable because spatial regions of high/low shading intensity are well defined across the year. For E/W PV, on

25

the other hand, the spatial shade homogeneity across the year makes it more similar to that for a traditional open agriculture with a reduced sunlight.

Finally, we would like to mention some economic factors which are although important, were deemed beyond the scope for this paper. First, since the bifacial solar panels can be somewhat more expensive, the levelized cost of energy (LCOE) for the energy system could be impacted by this [17]. The vertical tilt for the panels, on the other hand, is known to have a significantly reduced soling (dust accumulation) losses as compared to the tilted panels [16]. This can be particularly advantageous for AV application where a high dust environment is expected, especially during tillage and harvest seasons [13]. This implies that vertical panels may have a much less frequent cleaning requirement in AV farm as compared to the tilted panels. Since cleaning has its own cost associated with it, trade-off between a higher panel cost for bifacial panels vs. low cost of cleaning needs to be carefully examined to find an overall effect on LCOE. Nevertheless, with better land productivity, higher spatial uniformity for sunlight and associated water distribution for the farm, and reduced soiling loss, E/W faced vertical bifacial panels seem to have a promising prospective for AV applications.

References

[1] H. Dinesh, J. M. Pearce, The potential of agrivoltaic systems, Renewable and Sustainable Energy Reviews 54 (2016) 299–308 (2016).

[2] A. Weselek, A. Ehmann, S. Zikeli, I. Lewandowski, S. Schindele, P. Högy, Agrophotovoltaic systems: applications, challenges, and opportunities. a review, Agronomy for Sustainable Development 39 (4) (2019) 35 (2019).

[3] R. Mead, R. Willey, The concept of a âĂŸland equivalent ratioâĂŹand advantages in yields from intercropping, Experimental Agriculture 16 (3) (1980) 217–228 (1980).

[4] D. Majumdar, M. J. Pasqualetti, Dual use of agricultural land: Introducing 'agrivoltaics' in phoenix metropolitan statistical area, usa, Landscape and urban planning 170 (2018) 150–168 (2018).

[5] G. A. Barron-Gafford, M. A. Pavao-Zuckerman, R. L. Minor, L. F. Sutter, I. Barnett-Moreno, D. T. Blackett, M. Thompson, K. Dimond, A. K. Gerlak, G. P. Nabhan, et al., Agrivoltaics provide mutual benefits across the food–energy–water nexus in drylands, Nature Sustainability (2019) 1–8 (2019).

[6] C. Dupraz, H. Marrou, G. Talbot, L. Dufour, A. Nogier, Y. Ferard, Combining solar photovoltaic panels and food crops for optimising land use: towards new agrivoltaic schemes, Renewable energy 36 (10) (2011) 2725–2732 (2011).

[7] H. Marrou, L. Guilioni, L. Dufour, C. Dupraz, J. Wéry, Microclimate under agrivoltaic systems: Is crop growth rate affected in the partial shade of solar panels?, Agricultural and Forest Meteorology 177 (2013) 117–132 (2013).

[8] Y. Elamri, B. Cheviron, J.-M. Lopez, C. Dejean, G. Belaud, Water budget and crop modelling for agrivoltaic systems: Application to irrigated lettuces, Agricultural water management 208 (2018) 440–453 (2018).

[9] A. Goetzberger, A. Zastrow, On the coexistence of solar-energy conversion and plant cultivation, International Journal of Solar Energy 1 (1) (1982) 55–69 (1982).

[10] C. Dupraz, G. Talbot, H. Marrou, J. Wery, S. Roux, F. Liagre, et al., To mix or not to mix: evidences for the unexpected high productivity of new complex agrivoltaic and agroforestry systems, in: Proceedings of the 5th world congress of conservation agriculture: Resilient food systems for a changing world, 2011 (2011).

[11] P. R. Malu, U. S. Sharma, J. M. Pearce, Agrivoltaic potential on grape farms in india, Sustainable Energy Technologies and Assessments 23 (2017) 104–110 (2017).

[12] S. Amaducci, X. Yin, M. Colauzzi, Agrivoltaic systems to optimise land use for electric energy production, Applied energy 220 (2018) 545–561 (2018).

[13] T. Sekiyama, A. Nagashima, Solar sharing for both food and clean energy production: Performance of agrivoltaic systems for corn, a typical shade-intolerant crop, Environments 6 (6) (2019) 65 (2019).

[14] E. H. Adeh, J. S. Selker, C. W. Higgins, Remarkable agrivoltaic influence on soil moisture, micrometeorology and water-use efficiency, PloS one 13 (11) (2018) e0203256 (2018).

[15] M. R. Khan, A. Hanna, X. Sun, M. A. Alam, Vertical bifacial solar farms: Physics, design, and global optimization, Applied energy 206 (2017) 240–248 (2017).

[16] A. Ullah, H. Imran, Z. Maqsood, N. Z. Butt, Investigation of optimal tilt angles and effects of soiling on pv energy production in pakistan, Renewable energy 139 (2019) 830–843 (2019).

[17] M. T. Patel, M. R. Khan, X. Sun, M. A. Alam, A worldwide cost-based design and optimization of tilted bifacial solar farms, Applied Energy 247 (2019) 467–479 (2019).

[18] J. Appelbaum, Bifacial photovoltaic panels field 85 (2016) 338–343 (2016).

[19] I. Reda, A. Andreas, Solar position algorithm for solar radiation applications, Solar energy 76 (5) (2004) 577–589 (2004).

[20] PV performance modeling collaborative | an industry and national laboratory collaborative to improve photovoltaic performance modeling, `https://pvpmc.sandia.gov/`, [Online; accessed 19-September-2019] (2016).

[21] B. Haurwitz, Insolation in relation to cloudiness and cloud density, Journal of Meteorology 2 (3) (1945) 154–166 (1945).

[22] B. Haurwitz, Isolation in relation to cloud type, Journal of Meteorology 5 (3) (1948) 110–113 (1948).

[23] J. Orgill, K. Hollands, Correlation equation for hourly diffuse radiation on a horizontal surface, Solar energy 19 (4) (1977) 357–359 (1977).

[24] J. A. Duffie, W. A. Beckman, Solar engineering of thermal processes, Wiley New York, 1991 (1991).

[25] N. Martín, J. Ruiz, Annual angular reflection losses in pv modules, Progress in Photovoltaics: Research and Applications 13 (1) (2005) 75–84 (2005).

[26] M. F. Modest, Radiative heat transfer, Academic press, 2013 (2013).

[27] M. Cossu, L. Ledda, G. Urracci, A. Sirigu, A. Cossu, L. Murgia, A. Pazzona, A. Yano, An algorithm for the calculation of the light distribution in photovoltaic greenhouses, Solar Energy 141 (2017) 38–48 (2017).

[28] T. O. Kaddoura, M. A. Ramli, Y. A. Al-Turki, On the estimation of the optimum tilt angle of pv panel in saudi arabia, Renewable and Sustainable Energy Reviews 65 (2016) 626–634 (2016).

[29] H. Khorasanizadeh, K. Mohammadi, A. Mostafaeipour, Establishing a diffuse solar radiation model for determining the optimum tilt angle of solar surfaces in tabass, iran, Energy Conversion and Management 78 (2014) 805–814 (2014).